Breakdown Phenomenon and Electrical Process in a Microplasma System with InP Electrode

H. HILAL KURT[1,3] and B.G. SALAMOV[1,2]

1.—Department of Physics, Faculty of Science, Gazi University, 06500 Teknikokullar, Ankara, Turkey. 2.—Azerbaijan Academy of Science, Institute of Physics, 0143 Baku, Azerbaijan. 3.—e-mail: hkurt@gazi.edu.tr

The electrical characteristics of InP have been investigated experimentally and its electron density and electrical potential evaluated theoretically using the finite element method in a two-dimensional (2D) medium. Higher ionization rates were achieved at 39.99 kPa and 450 V, and the maximum electron density in the cell was found to lie around $\sim 8.64 \times 10^{23}$ m^{-3}. The main motivation for the use of InP electrodes is the promising optoelectronic characteristics of this material. The plasma currents and gas discharge emissions were recorded simultaneously for an InP electrode under air or He medium. The breakdown voltage was investigated under various operating conditions including He and air plasma. Use of air resulted in a better minimum breakdown point compared with He; that is, the minimum voltage was reached at lower pressure, viz. p = 3.73 kPa for air versus p = 25.99 kPa for He. The system was found to depend on the pressure of the cell, with a transition occurring from the Townsend to glow mode. Self-sustained discharge contributed to the current–voltage characteristics and light emission over a wide pressure range between 1.99 kPa and 101.325 kPa for various interelectrode gaps. It has been shown that the intensity of the plasma is higher in air than He, being 10 a.u. for air versus about 5 a.u. for He under the same conditions.

INTRODUCTION

Over recent years, research into group III–V semiconductor materials has progressed significantly in terms of understanding their physical and optical processes.[1–4] Moreover, there is a growing need for such semiconductor materials for use in high-speed multifunctional systems in the electronics and optics fields.[1] InP-based materials have always been a focus of research for the following reasons[1–8]: Indium phosphide (InP) exhibits very high current and discharge emission due to its direct bandgap of 1.34 eV at room temperature,[6–10] making it a perfect candidate for use in optoelectronics systems that involve a plasma. Notably, great research effort has focused on alloy semiconductors composed of various compound semiconductors. The most widely known group III–V compound semiconductors are GaAs, InP, GaN, and AlN,[11] among which the composition ratio can be changed continuously.[11] Based on these advantages, group

III–V materials represent a flexible set of materials that are well suited to use in optoelectronic applications. These characteristics also make them appropriate materials for use in efficient solar cells. Their flexible spatial features enable the exploration of new designs,[12] but a single direct-bandgap material system cannot cover a wide range of the optical spectrum; For example, GaAs and indium phosphide (InP), and their triple and quadruple alloys, can be used in different telecommunications windows extending in the infrared from wavelengths of 750 nm to 1700 nm.[11,12]

In semiconductors, an electronic bandgap forms as a result of scattering of electrons by atoms at crystallographic lattice points separated by a few nanometers. The width of the bandgap plays a decisive role in the transport mechanism that is exhibited when an external electric field is applied to the material or it is stimulated optically. When the light that hits a material has sufficiently high energy compared with the width of the forbidden

bandgap, energetic electrons can transition from the valance band (which is completely full of electrons at 0 K) to the conduction band (which can be considered to be completely devoid of electrons at 0 K) as a result of the photoeffect in semiconductors. In this way, the carrier concentration and conductivity of a material can be controlled depending on the energy of the incoming light. Moreover, group III–V materials are the strongest candidates for use in optoelectronic devices that should exhibit optical gain.[2] Although offering high performance that is comparable to other group III–V materials, InP is known for its efficient operation, which is attributed to its carrier dynamics related to its high electron mobility in the transport mechanism.

Study of the discharges that occur across gaps of micron size at low temperatures is of great interest for plasma light sources, too. When the currents formed by ions and electrons are sufficiently high, the resulting ionized gas may emit light in the visible range. On the other hand, secondary-electron emission can also take place from the cathode, and these electrons are mainly associated with the positive charges that accumulate in front of the cathode over a wide range of operating conditions. When ions strike the cathode, secondary electrons are produced then accelerated towards the anode, contributing to the ionization by colliding with gas atoms. As a result of these multiplication ionization processes, breakdown, i.e., a self-sustaining discharge, occurs in the plasma cell and external ionization is not necessary for a discharge current to flow.[13,14] The critical breakdown voltage (V_B) at which this occurs is a function of the product of the pressure p and the interelectrode distance (d). This is known as Paschen's law, which can be used to determine the optimum pressure and voltage required to initiate such gas discharge. When the conditions for breakdown are fulfilled, discharge can be sustained, as described by Paschen curves, which can be obtained for the ionization of different gases.[13,14]

This study includes experimental measurements of current–voltage characteristics (CVC) and discharge light emission (DLE) curves using a microplasma cell and calculations of the electron density using COMSOL Multiphysics software. The electron density at different pressures and voltages are compared. The results of the numerical simulations allow the unspecified parameters to be found. The experimental section presents a detailed analysis of the discharge for air and He media, as well as the corresponding Paschen curves. InP exhibits remarkable plasma currents and plasma emission in the proposed structure.

EXPERIMENTAL PROCEDURES

In this study, a commercial semiinsulating Fe-doped InP (001) wafer was used as the cathode material in the plasma cell. On top of the InP, a Au contact (40 nm) was deposited under high-vacuum condition using an evaporation system. Thin-film covered SnO_2 was used as the anode. The resistivity of InP is in the order of 10^7 Ω cm. The measurements were conducted in a microplasma laboratory using a vacuum of up to 0.013 kPa. He or air was used as the gas medium between the electrodes. A power supply of 2.5 kV was provided to drive the electrons through the cell. The maximum current was around 10^{-4} A. The experimental setup is shown schematically in Fig. 1. The electrodes were connected to the power supply system. The gas discharge process was carried out at fixed interelectrode distance but varying voltages and pressure values. To measure the Paschen curves, a direct-current (DC) microdischarge system was used with a 10 kΩ resistor connected in series. The gas discharge characteristics of the plasma were measured using a Keithley 199 multimeter and digitalized using custom-made software in a personal computer (PC). The pressure in the discharge cell was adjusted using a digital vacuum gate. The width of the gap was set to 30 μm to 550 μm based on the thickness of insulating mica foils.

THEORETICAL RESULTS

The COMSOL Multiphysics package was used to model the semiconductor–plasma structure. Numerical simulation is an indispensable tool to understand the behaviour of the plasma inside a microdischarge cell with an InP electrode and is also vital to improve knowledge in the field of DC discharge, which is used for deposition or etching.[17–19] The optimal mesh with 42,560 elements was applied. The system used the gas discharge formalism and the required material constants to obtain steady-state solutions for the defined simulation cell.[20,21] Note that only limited theoretical studies on the transport properties of group III–V semiconductors are available.

The electron density in the plasma was calculated using COMSOL simulation software. The electron density and potential distribution maps were obtained by considering successive ionizing collisions between ions, electrons, and neutral atoms, taking into account the diffusion equation per species based on the ionization rate per species and the electrostatic potential solution. The electrons were mostly concentrated in the central region of the cell, although some diffused to both ends of the cell (Fig. 2a); that is, because of the potential surface difference, the electron distribution changed drastically. In Fig. 2a, the electrons are seen to accumulate mostly in the middle of the cell. However, two electron structures were observed at the slightly higher pressure of $p = 39.99$ kPa (Fig. 2b). Depending on the discharge conditions, the electron distribution is concentrated at different locations within the plasma region, as shown by the different plasma discharge zones observed in Fig. 2a–d.
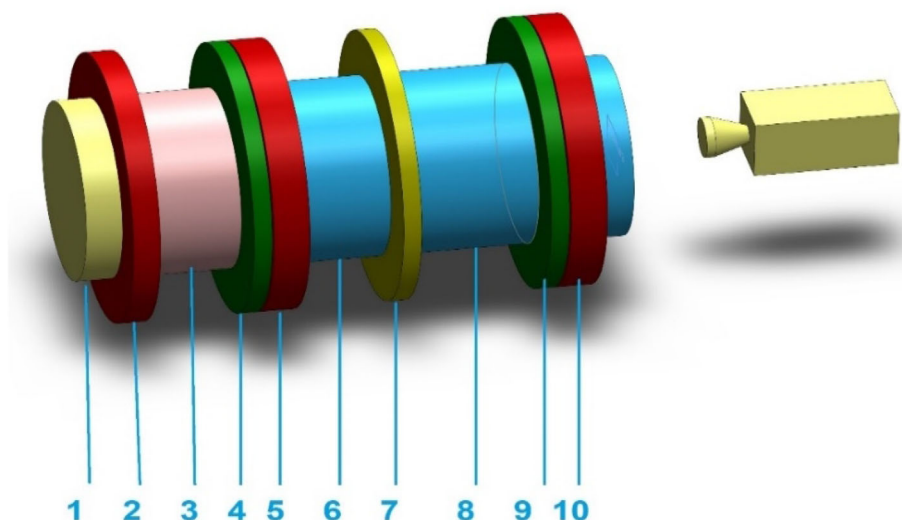
Fig. 1. Microdischarge cell with one discharge gap: 1, light source; 2, Si filter; 3, IR light beam; 4, semitransparent Au contact; 5, InP electrode; 6, gas discharge gap filled by air; 7, mica foil; 8, UV–Vis light beam; 9, transparent conductive SnO_2 electrode; 10, flat glass disc[15,16].

Considering the electron distribution in Fig. 2, the steady-state solution depends drastically on the potential and pressure.

The electron density distribution was obtained at a fixed gap of 50 μm. Maximum electron density values of 3.18 $\times$ 10^{22} m^{-3}, $\sim$ 8.64 $\times$ 10^{23} m^{-3}, 2.81 $\times$ 10^{22} m^{-3}, and 3.25 $\times$ 10^{22} m^{-3} were calculated for the different pressure levels in various parts of the plasma cell. In addition, as the voltage was increased, so did the electron density.

However, the degree of ionization increased depending on both the pressure and voltage, with the highest electron density being reached for 39.99 kPa and 450 V (Fig. 2). The electron density in the discharge is one of the key parameters of the process. As shown in Fig. 2a–d, the electron density was not constant but rather changed on increasing the voltage applied across the cell. The location of the electron density depends on the plasma conditions such as the pressure, electric field strength, interelectrode distance, and a power. When the pressure in the chamber changes, the location of the electron density also changes strongly.

When the voltage changes, the potential increases as expected and a smooth potential curve is observed for high-voltage excitation (Fig. 3c). For low-voltage cases, a small and moderate valley is seen around the cathode (Fig. 3a, and b).

As the voltage changes, the potential distribution also changes. This may be due to the redistribution of the electric field according to the mean energy of the electrons in the plasma. Furthermore, it is assumed that the distribution of the potential during the evolution of the discharge is governed by the energetic electrons generating in the cathode–anode gap. The dynamics of the plasma are determined by the number of electrons generated during the avalanche mechanism occurring between the cathode and anode. Figure 3c shows a potential value of 1197.3 V, which is approximately four orders of magnitude larger than that in Fig. 3a.

EXPERIMENTAL RESULTS

The Paschen curves for the microgaps with an InP electrode were studied using the planar gas discharge system. The effects of the type of gas and the gap width as well as the discharge pressure on the Paschen's curve, were examined in detail. Figure 4 shows the dependence of the breakdown voltage on the pressure for Air or He plasma for different interelectrode distances d.

The influence of the type of gas on the CVC was also studied in the discharge chamber with a diameter of 50 mm for interelectrode distances of 50 μm and 100 μm. Figure 4 shows plots of the product pd, which is known as Paschen's law in plasma science, revealing that the breakdown voltage decreased to a minimum with increasing pressure, then increased with increasing pressure thereafter. This minimum indicates the optimal operating pressure and voltage for the microdischarge system. The type of gas is also seen to affect the breakdown process.

The minimum breakdown voltage shifted towards lower pressure for air compared with He; that is, the minimum breakdown point was seen at around 3.73 kPa for air but around 25.99 kPa for He. The threshold U_B voltage was measured to be 324 V and 282 V in the case of air and He, respectively.

Breakdown occurred at a lower voltage for 50 μm compared with the case of 100 μm. The Paschen curves showed different behavior for the systems with air and He plasma (Fig. 4). The discrepancy between the two Paschen curves appeared for larger pd values. The breakdown curves for the air
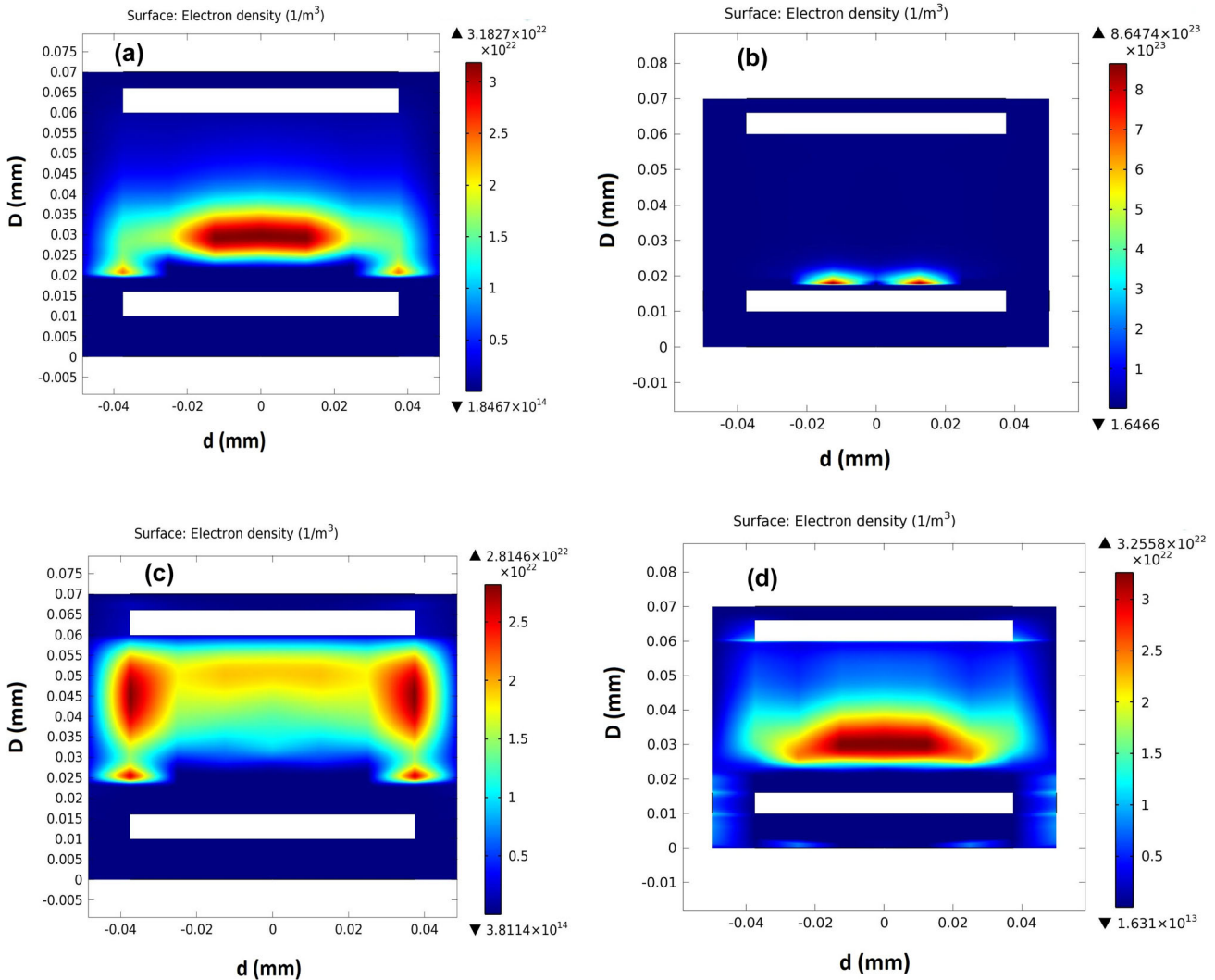
Fig. 2. Electron density maps computed using COMSOL M software. The color bar shows the magnitude of the electron density in units of m^{-3} under conditions of (a) 13.3 kPa and 450 V, (b) 39.99 kPa and 450 V, (c) 6.66 kPa and 2000 V, and (d) 13.3 kPa and 2000 V. The images show the electron distribution obtained in the 2D mode (Color figure online).

environment clearly show a U shape, while there is an obvious deviation from such a U shape on the right side of the Paschen curve for He.

Figure 5 shows the measured breakdown voltage as a function of the gas pressure for a microgap with different distances d when using He. The interelectrode space is divided into two distinct regions: A high-field ionization region surrounding the active electrode, where the free charges are produced (50 μm to 100 μm), and a low-field drift region beyond $d = 100$ μm. These low d values shifted the right part of the axis. However, the breakdown curves demonstrated a similar behavior in the interelectrode range of 240 μm to 540 μm. Comparison of the curves shows that the optimal interelectrode distance in the cell was 240 μm. Even when increasing d further, the minimum point remained

nearly at the same value of around 8.79 kPa for 240 μm to 540 μm. It can be seen that the breakdown (U_{B}) curves showed a sharp and strong decrease with respect to pressure in the ionization region after 100 μm. In addition, the curves reached the same U_{B} values at higher pressures after 400 V, as shown in Fig. 5. For the low value of d, the breakdown curves demonstrated a smooth variation with p. In all cases, the space charge accumulation around the cathode was neglected. The distance between the electrodes affected the breakdown voltage, and the experimental curves confirmed Paschen's law, with a minimum point indicating the optimum plasma conditions.

Our previous work[21] concluded that the interelectrode distance played a major role in the discharge volume during the breakdown process; however, the
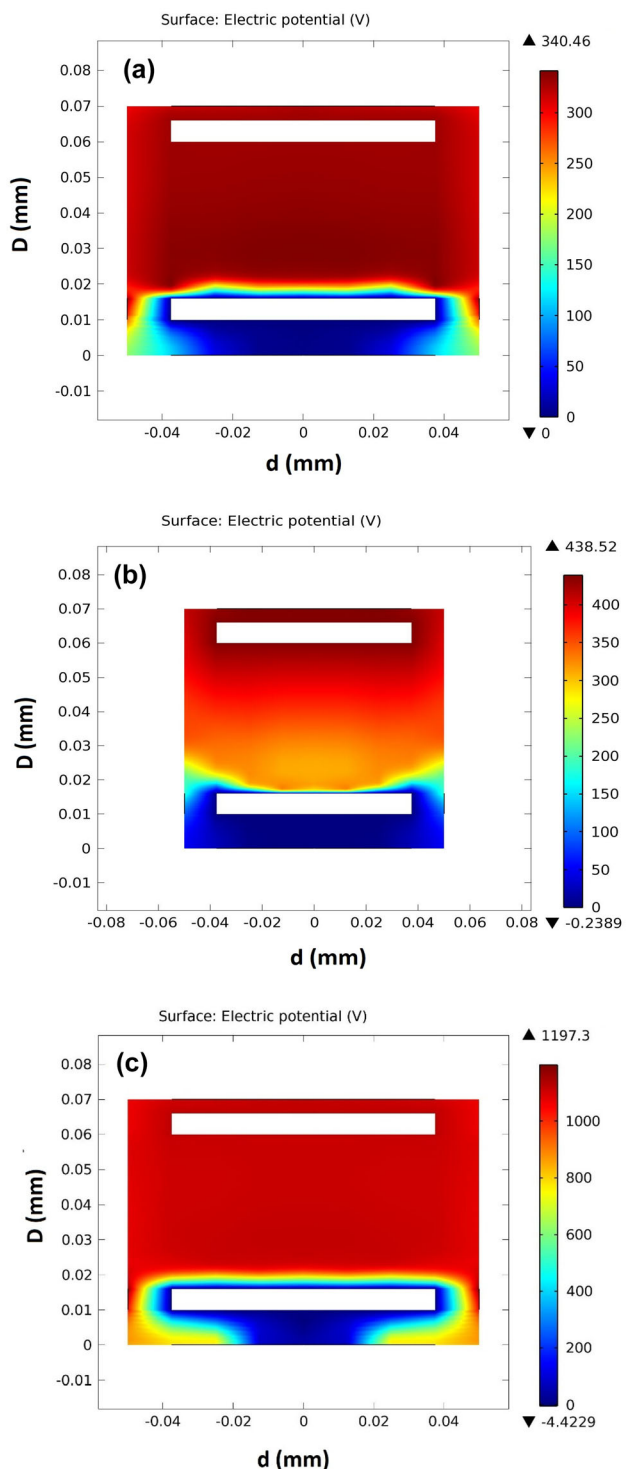
Fig. 3. DC plasma potential maps. The magnitude of the floating potential is shown by the color bar, expressed in volts, under conditions of (a) 13.33 kPa and $U = 450$ V, (b) 101 kPa and $U = 450$ V, and (c) 13.33 kPa and $U = 2000$ V (Color figure online).

Fig. 4. Breakdown curves in air and helium for (a) 100 μm and (b) 50 μm. D is the diameter of the InP electrode.
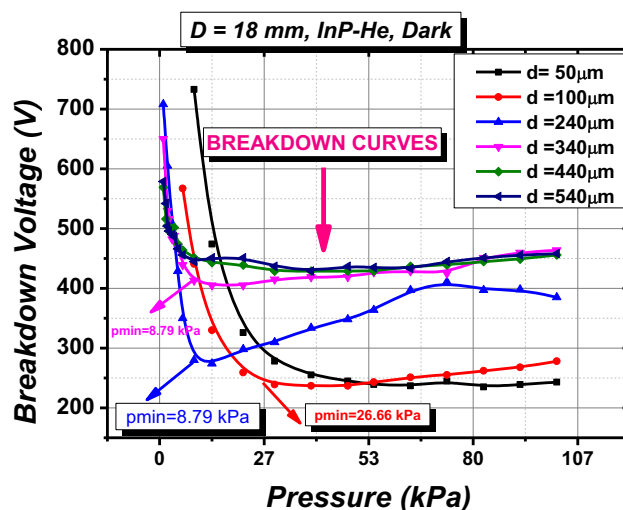
Fig. 5. Experimental breakdown curves as a function of interelectrode distance d in He.

type of gas is also very important for enhanced secondary-electron emission, causing a reduction in the minimum point in the Paschen curves.
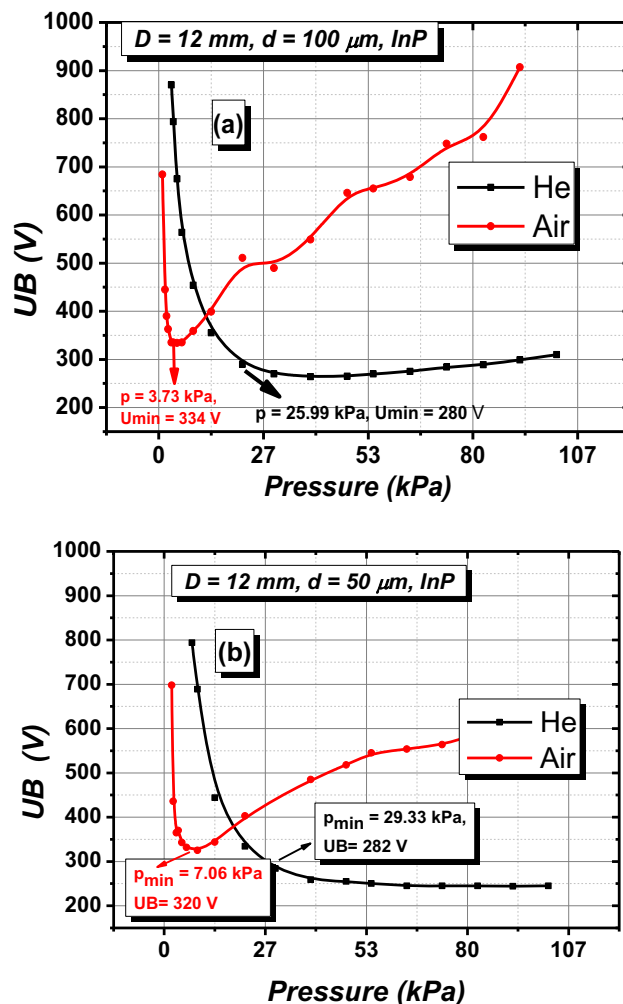
Very few electron–ion collisions occur in the plasma in the low pressure ranges, while the number of secondary electrons generated is too low to sustain ionization in the discharge cell. Meanwhile, frequent collisions occur at higher pressure values, but the electrons do not obtain sufficient energy to ionize gas atoms, thus the discharge is quenched and nonsustainable.[22–25] Thus, in both situations, the ion production rates are low and high voltages are required to provide discharge.

On the right side of the Paschen curve, the breakdown voltage U_B shows a proportional increase with pd. This is due to the fact that the probability of an electron producing ionization is very high for relatively large pd values, even in a moderately reduced electric field E/p. On the left, the voltage U_B increases sharply when pd decreases. Higher electric fields are thus needed, because low pd values are less likely to result in ionization due to the small number of ionizing collisions of electrons on the left-hand side of the curve. Therefore, the Paschen curve shows a minimum point where the ionization probabilities of the electrons are maximum and the optimal conditions to sustain the gas discharge are obtained.

The electron discharge emissions and current–voltage characteristics in the plasma discharge are plotted as a function of the interelectrode distance d and gas pressure p in Fig. 6. It is shown that the

discharge in air exhibits better CVC and DLE values for all the studied pressures. On the other hand, the uniformity of the light emission depends on the resistivity distribution of the photodetector plate and is proportional to the discharge current, with local changes in the resistivity of the photodetector (InP electrode) leading to local changes in the current and gas discharge emission.

These results reveal that the CVC and DLE show similar behavior in the same experimental parameter range due to the ionization process from the cathode to anode. Consequently, increases in the electric field strength as well as the electron density contribute to the high current and discharge emission in the plasma cell. The CVC and DLE depend directly on the quality of the wafer. Therefore, any relevant evaluation of the quality of the material requires a description of the spatial distribution of both electrical parameters and structural defects. If the electrode has uniform resistivity, the plasma becomes uniform. However, if the electrode contains natural defects such as EL2 (native trap) centers or impurities due to the growth conditions applied, instabilities such as negative differential resistance or fluctuations will be recorded in the plasma cell. In the absence of a sufficient electric field, the plasma should sustain Townsend breakdown via secondary electrons. When the plasma current increases in the cell, the effect of space charge on the uniformity of
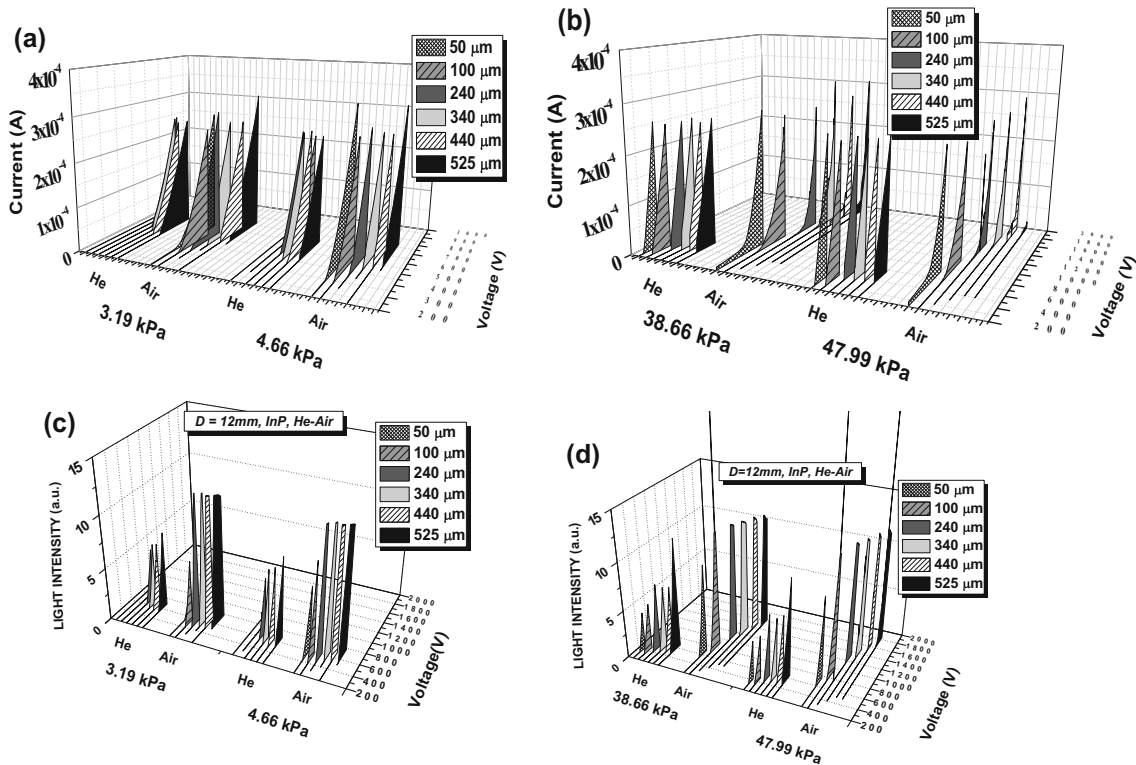

Fig. 6. Variation of discharge current and discharge emission with pressure for different electrode separations in different pressure regimes: (a) CVCs for 3.19 kPa and 4.66 kPa, (b) CVCs for 38.66 kPa and 47.99 kPa, (c) DLEs for 3.19 kPa and 4.66 kPa, and (d) DLEs for 38.66 kPa and 47.99 kPa.

the electric field will become important and distort the homogeneity of the electric field between the electrodes, resulting in a contraction of the gas discharge. As a result of this, the CVC tends to go negative in this mode, leading to current instabilities in the system. The discharge is now in glow mode, where the current is in the order of 10^{-4} A to 10^{-1} A and the discharge light emission is brighter than in the Townsend mode.[23–25]

The properties of the glow discharge change in accordance with the discharge parameters such as the gas pressure, plasma gas composition, gas pressure, and voltage applied across the electrodes. The composition of the plasma gas is particularly important for the excitation and ionization mechanisms, including the production of active species.[26]

CONCLUSION

The influence of the type of gas on the breakdown voltage has been studied theoretically and experimentally, as well as the influence of the pressure and interelectrode distance d on the CVCs and DLEs. The cell operating with He showed a smooth dependence on p, whereas the curves obtained with air showed a sharp dependence on p. Furthermore, electron distribution and potential maps were calculated theoretically, considering the redistribution of the electric field in the cell. This provides information regarding the appearance of the gas discharge across the gap when a potential is applied to the cell. The properties of the DC plasma were studied using COMSOL software for different input voltage and pressure settings. The theoretical electron density changed from 3.18×10^{22} m^{-3} to 8.64×10^{23} m^{-3}. These values confirm that the "dense plasma" condition is valid within the specified parameter range. The peak plasma density was 8.64×10^{23} m^{-3} at 39.99 kPa and 450 V. The electron density depends on the gas pressure and applied voltage in the interelectrode area. Some distinctive features of the electron density in the plasma system with the InP electrode are clarified by these results, considering the electron ionization and emission from the cathode. Furthermore, an increase in the bias voltage at a constant gap distance can effectively enhance the electric field and electron density and also provide more energy to electrons, consequently leading to high discharge emission from the cell.

REFERENCES

1. Z. Mia and Y.L. Chang, *J. Nanophotonics* 3, 031602 (2009).
2. S.J. Sweeney and J. Mukherjee, *Optoelectronic Devices and Materials* (Springer Handbook of Electronic and photonic Material, 2017).
3. R.I. Dzhioev, B.P. Zakharchenya, and V.G. Fleisher, *JETP Lett.* 14, 381 (1971).
4. C. Caspers and J.P. Ansermet, *Appl. Phys. Lett.* 105, 133110 (2014).
5. T.P. Pearsall, eds., *Properties, Processing and Applications of Indium Phosphide, IEE/INSPEC* (London: The Institution of Electrical Engineers, 2000).
6. R.A. Stradling and P.C. Klipstein, *Growth and Characterisation of Semiconductors* (Bristol and New York: Adam Hilger, 1990).
7. D. Dupont, M.D. Tessier, P.F. Smet, and Z. Hens, *Adv. Mater.* 29, 1700686 (2017).
8. F. Zafar and A. Iqbal, *Proc. R. Soc. A* 472, 0804 (2015).
9. Y. Song, L. Cao, B.D. Peng, G.Z. Song, Z.Q. Yue, J.M. Ma, L. Sheng, B.K. Li, and H.X. Wang, *Rev. Sci. Instrum.* 88, 033109 (2017).
10. V. Dhaka, V. Pale, V. Khayrudinov, J.P. Kakko, T. Haggren, H. Jiang, E. Kauppinen, and H. Lipsanen, *Nanotechnology* 27, 505606 (2016).
11. H. HayasHi, in *Development of Compound Semiconductor Devices*. Search of Immense Possibilities (2011).
12. S. Fathpour, *Nanophotonics* 4, 143 (2015).
13. YuP Raizer, *Gas Discharge Physics* (Berlin: Springer, 1997).
14. M.C. Penache, *Study of High-Pressure Glow Discharges Generated by Micro-Structured Electrode (MSE) Arrays*. Dissertation zur Erlangung des Doktorgrades der Naturwissenschaften vorgelegt beim Fachbereich Physik der Johann Wolfgang Goethe Universität in Frankfurt am Main, 2002.
15. H. Hilal Kurt, *J. Electron. Mater.* 47, 4486 (2018).
16. H. Hilal Kurt, E. Tanrıverdi, and B.G. Salamov, *JOM* 71, 644 (2019).
17. D. Benyoucef, *Modélisation Particulaire et Multidimensionnelle des Décharges Hors Equilibre à Basse Pression Excités par Champs Electromagnétiques*. Ph.D. dissertation, Dept Elect. Eng, Toulouse III – Paul Sabatier Univ, May 2011.
18. J. van Dijk, G.M.W. Kroesen, and A. Bogaerts, *J. Phys. D Appl. Phys.* 42, 190301 (2009).
19. M. El Bojaddaini, H. Chatei, M. Atounti, M. El Haim, I. Driouch, and M. El Hammouti, *Appl. Math. Sci.* 6, 6003 (2012).
20. J.D. Freels and P.K. Jain, in *COMSOL Conference Proceedings* (2011).
21. Y. Sadiq, H. Yücel-Kurt, A.O. Albarzanji, S.D. Alekperov, and B.G. Salamov, *Solid State Electron.* 53, 1009 (2009).
22. M. Ohring, *Materials Science of Thin Films*, 2nd edn, ISBN: 9780080491783 (Academic: 15 October 2001), p. 794.
23. V.I. Kolobov and A. Fiala, *Phys. Rev. E* 50, 3018 (1994).
24. R. Arslanbekov and V. Kolobov, *J. Phys. D Appl. Phys.* 36, 2986 (2003).
25. M.T. Jamil, J. Ahmad, S.H. Bukhari, M.E. Mazhar, U. Nissar, A.J. Rao, H. Ahmad, and G. Murtaza, *Dig. J. Nanomater. Biostruct.* 12, 595 (2017).
26. Y. Fu, P. Zhang, and J.P. Verboncoeur, *Appl. Phys. Lett.* 113, 054102 (2018).